Check for updates

Received: 9 March 2021 | Revised: 19 July 2021 | Accepted: 19 July 2021

DOI: 10.1002/mp.15135

MEDICAL PHYSICS

SPECIAL ISSUE PAPER

FLASH radiotherapy with carbon ion beams

Uli Andreas Weber[1] | **Emanuele Scifoni**[2] | **Marco Durante**[1,3]

[1]Biophysics Department, GSI Helmholtzzentrum für Schwerionenforschung, Darmstadt, Germany

[2]Istituto Nazionale di Fisica Nucleare (INFN), Trento Institute for Fundamental Physics and Applications (TIFPA), Trento, Italy

[3]Institute of Condensed Matter Physics, Technische Universität Darmstadt, Darmstadt, Germany

Correspondence
Prof. Marco Durante, PhD, Biophysics Department, GSI Helmholtzzentrum für Schwerionenforschung, Planckstraße 1 - 64291 Darmstadt, Germany.
Email: m.durante@gsi.de

Funding information
Istituto Nazionale di Fisica Nucleare (INFN); FAIR Phase-0; GSI HELMHOLTZZENTRUM FUR SCHWERIONENFORSCHUNG GMBH

Abstract

FLASH radiotherapy is considered a new potential breakthrough in cancer treatment. Ultra-high dose rates (>40 Gy/s) have been shown to reduce toxicity in the normal tissue without compromising tumor control, resulting in a widened therapeutic window. These high dose rates are more easily achievable in the clinic with charged particles, and clinical trials are, indeed, ongoing using electrons or protons. FLASH could be an attractive solution also for heavier ions such as carbon and could even enhance the therapeutic window. However, it is not yet known whether the FLASH effect will be the same as for sparsely ionizing radiation when densely ionizing carbons ions are used. Here we discuss the technical challenges in beam delivery and present a promising solution using 3D range-modulators in order to apply ultra-high dose rates (UHDR) compatible with FLASH with carbon ions. Furthermore, we will discuss the possible outcome of C-ion therapy at UHDR on the level of the radiobiological and radiation chemical effects.

KEYWORDS
C-ions, dose rate, FLASH, heavy ion therapy, scanning

1 | INTRODUCTION

The effect of high dose rates in mammalian cells has been investigated for many years.[1,2] However, the idea to apply ultra-high dose rates (UHDR) to radiotherapy has been triggered by recent pre-clinical experiments using electrons in animal models.[3,4] A Franco-Swiss team convincingly showed that at dose rates exceeding at least 40 Gy/s the tumor control was similar to conventional intensities, but had much lower normal tissue toxicity, thus widening the therapeutic window. The results have been subsequently confirmed by other investigators[5–7] and clinical trials are starting using electrons or protons. In fact, it is hard to reach the UHDR necessary for triggering FLASH effects using conventional X-rays from LINACS. The pre-clinical studies focused on electrons from LINACS, protons from cyclotrons, and X-rays produced by synchrotron radiation sources. But now, the interest of research is shifting increasingly toward the clinical transfer of FLASH.

Carbon ion-beam treatment, moreover, is a less frequently applied (compared to the previously mentioned therapy forms) but continuously growing modality for particle therapy, exploiting physical[8,9] and biological[10] properties of densely ionizing (high-LET) radiation. Presently there are a dozen C-ion therapy centers worldwide and many phase II/III comparative clinical trials ongoing.[11] Use of ions heavier than carbon (up to neon) was attempted in the Lawrence Berkeley Laboratory clinical trial,[12] but produced high toxicities. If a FLASH effect could also be observed for carbon ions, it would provide a large benefit for this modality and could pave the way to the use of ions beam with $Z > 6$ against radioresistant, hypoxic tumors.

This is an open access article under the terms of the Creative Commons Attribution License, which permits use, distribution and reproduction in any medium, provided the original work is properly cited.
© 2021 The Authors. *Medical Physics* published by Wiley Periodicals LLC on behalf of American Association of Physicists in Medicine.

However, FLASH effect investigations with C-ions presents technological and scientific questions. From the technological point of view, C-ion therapy is based on synchrotrons, where UHDR are more difficult to achieve than with cyclotrons used in proton therapy. Moreover, dosimetry must be accurate and avoid saturation at dose rates much higher than in conventional therapy. A further issue is the beam application, which must be performed within a few hundred milliseconds in order to reach FLASH conditions with UHDR. The standard multi-energy scanning technique and the corresponding energy switching times are clearly too slow for FLASH.[13]

As the FLASH effect is likely to depend strongly not only on dose rate but also on the beam characteristics,[14,15] these aspects will have an impact on scientific results, too. From a scientific aspect, the question is whether the FLASH effect will be visible also with densely ionizing heavy ions. First experiments showing the FLASH effect were interpreted using the oxygen depletion hypothesis,[16–19] a hypothesis that was recently challenged (see Section 2), and it is well-known that densely ionizing radiation-induced effects are less dependent on oxygen concentration than X-rays.[20] Simulations of oxygen generations in tracks suggest that C-ions may elicit a FLASH effect,[21,22] yet differently as compared to conventional radiation. The verification of the FLASH effect with C-ions will also help clarify the mechanism itself.

Thus, while radiobiological experiments with C-ions are highly anticipated, in order to prepare the ground for such investigations, in this paper we will first review possible FLASH effects connected to the specific radiation quality of carbon ion beams (Section 2), and then we will discuss the technical challenges in realizing a UHDR irradiation with carbon beams (Section 3). A concept for applying UHDR irradiations with 3D range modulators[23] will be presented; furthermore, the feasibility for FLASH application dependence on the tumor size and the available beam intensity of the accelerator will be assessed with some example treatment planning studies. In this context, the increased local dose rate due to beam scanning is also evaluated. Finally, we will discuss the future directions in high-LET FLASH research.

2 | EXPECTED FLASH EFFECT AT HIGH-LET

Predicting a FLASH effect following exposure to high dose rate carbon ions, as well as its variability across an irradiated field or dependence upon scanning and dosimetric parameters, is contingent on the normal tissue protective mechanism dependence on radiation LET. While the highest LET values will be mostly concentrated in the tumor regions, still, for carbon ions, the LET distribution in the normal tissue ranges between 10 and 50 keV/μm, values very far from that of low- or high-energy electrons as well as proton beams. This is without considering the distal fall-off regions, where eventually an organ at risk may lay, and where LET can be as high as 200 keV/μm. This is briefly illustrated in Figure 1, where a dose averaged LET profile (LETd) of a modulated carbon field (spread-out Bragg peak, optimized on RBE-weighted dose[24]) impinging on a box target centered at 80 mm depth (computed for a water phantom with the research treatment planning TRiP98[25,26] and LEM-IV[27] RBE tables for exemplary tumor and normal tissues both with α/β = 2 Gy, as in Ref. [28]) is compared to the corresponding, isorange, proton field. The different densities of the tracks on the nanoscale (20 nm box) are also shown for a depth

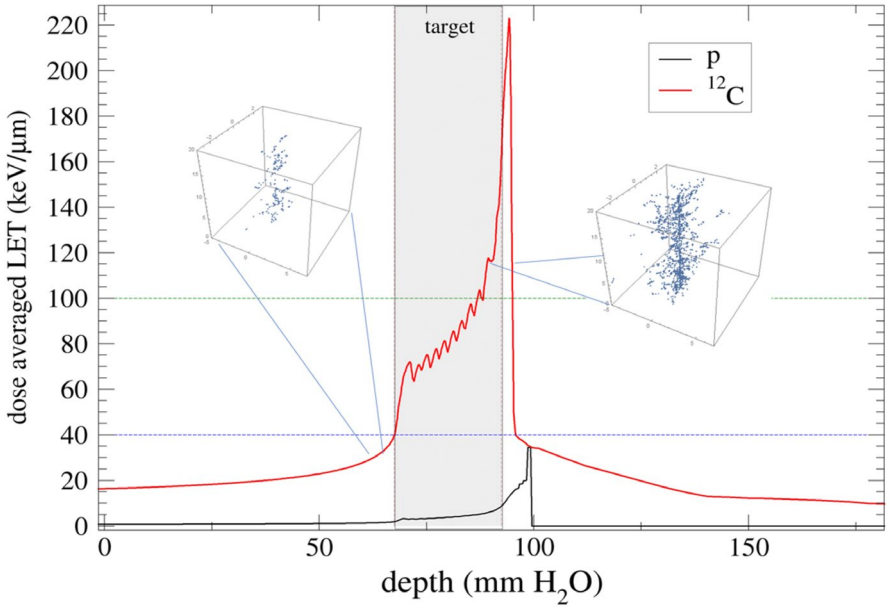

FIGURE 1 Typical dose averaged LET (LETd) profiles in water for a carbon ion field, as compared to a proton one, for a target at isodepth (computed with TRiP98). The horizontal lines at 40 and 100 keV/μm represent, respectively, the maximum LETd in the normal tissue entrance channel excluding the distal fall-off and a level where oxygenation effects are expected to saturate to negligible values. In the insets, ionization densities snapshot, in cubes of 20 nm for, respectively, 10 and 1 MeV/u carbon ions (computed with TRAX)

position right before the target and at the distal position (computed with TRAX[29]).

The LET dependence of the FLASH effect[22,30] hangs on the basic mechanism of FLASH, which is presently still far from being fully understood.

2.1 | Main mechanistic hypotheses on the FLASH effect

The biophysical modeling research has explored different pathways[15–18,31–39] for justifying the observations arising from the in vivo FLASH experiments.[3,4,6,40] Since pulse radiolysis experiments,[41] (from the nano- until the latest femto- and atto-chemistry studies[42]), the radiation chemistry community has been prompted to find an "ab initio" description of the spatio-temporal evolution of the UHDR physico-chemical processes. These investigations are feasible with the current experimental and theoretical tools.[43]

While the radiolytic oxygen depletion hypothesis (ROD) was initially believed as the major driving force[3,18,44] of the FLASH effect, possible alternative mechanisms[31,32,34,35,37,38,45,46] have been recently proposed, after several inconsistencies in the ROD hypothesis were shown. ROD seemed to be supported by the observed reduction of the FLASH effect, both in vitro[47–49] and in vivo,[6] when the oxygenation is increased. This hypothesis, suggesting transient hypoxia generated by the fast consumption of oxygen and consequently increased radioresistance, was initially proposed by Hall and Brenner,[44] and recently reformulated by Pratx,[18] and reported by several other authors.[15–17,50] However, recent reports challenged this simple explanation, showing an insufficient depletion in the typical doses used in preclinical experiments where the effect was, indeed, observed. In particular, most recent experimental and theoretical studies convene in estimating a depletion of 2.1%–2.5% pO_2 in 100 Gy.[32,37,45,46]

Other approaches are presently under study including differential redox response in tumor and normal cells in processing the radiation chemical damage,[34] recombination of radicals during the heterogeneous stage,[45] sparing of hypoxic stem cells niches,[51] DNA damage repair kinetics differences[39] and even immune system[38] driven pathways—recently challenged by the observation of FLASH effect also in nude mice.[7] See Ref. [43] for a very clear and systematic analysis of the possible approaches from the chemical point of view.

LET parameter consideration is of course part of such studies. However, the only study dedicated to C-ions up to now,[21] following an idea previously suggested,[22] points to an alternative FLASH effect, which instead of protecting the normal tissue (dose modifying factor, DMF(NT) <1), would rather enhance tumor control (DMF(T) >1). The ground for this argument was the reconsideration of the channel of double ionization inducing the generation of oxygen for densely ionizing radiation, which was at the basis of the so-called "oxygen in the track" hypothesis[52] that explains the reduction of OER at increasing LET. Thus, according to the authors, an additional generation of oxygen in the higher LET region (tumor) would increase and thus enlarge the therapeutic window in the absence of a protective effect in the normal tissue. As detailed there, clearly such an effect, being specific of highly dense tracks, loses its power at low LET, as in conventional proton irradiation.

The spatiotemporal scales of radiation damage compared to the length of a typical FLASH (UHDR) pulse are shown in Figure 2. In particular, the sequence of the different physical, chemical, and biological steps is illustrated.

At high LET all the steps will be importantly modified, arguably including the last biological stage, which despite being a tissue response, and thus more a target property than a feature connected to the beam delivery, is ostensibly dependent on radiation quality.[10] Moreover, the biochemical stage is also dramatically affected by the radiation track structure. Thus, many of the above-mentioned hypothesized mechanisms will be impacted by the LET radiation features. As we partially will show below, it is expected in any case that this impact of higher LET will be detrimental for realizing the UHDR conditions.

2.2 | Impact on oxygenation

It is well known that high LET reduces the impact of variable oxygenation on the sensitivity of an irradiated tissue. Such an effect has been extensively observed experimentally and investigated theoretically.[54,55]

Under the ROD hypothesis, it would be expected that increasing LET should suppress the FLASH effect, for at least two reasons. First, as mentioned above higher LET correlates with strongly reduced sensitivity to oxygen concentration, leveling out substantially the OER effect.[54,55] For the same oxygenation level, thus an eventual oxygen depletion would have a sensibly lower impact on the OER.

Second, as shown in our previous work,[37] using the Monte Carlo chemical track structure code TRAX-CHEM,[56] the oxygen depletion at high-LET should require much larger doses, since denser ionization tracks lead to the intra-track recombination of radicals (see Section 2.3) suppressing the typical processes consuming oxygen, shown by the following chemical reactions:

$$e_{aq}^{-} + O_2 \rightarrow O_2^{\bullet -},$$

$$H^{\bullet} + O_2 \rightarrow HO_2^{\bullet}.$$

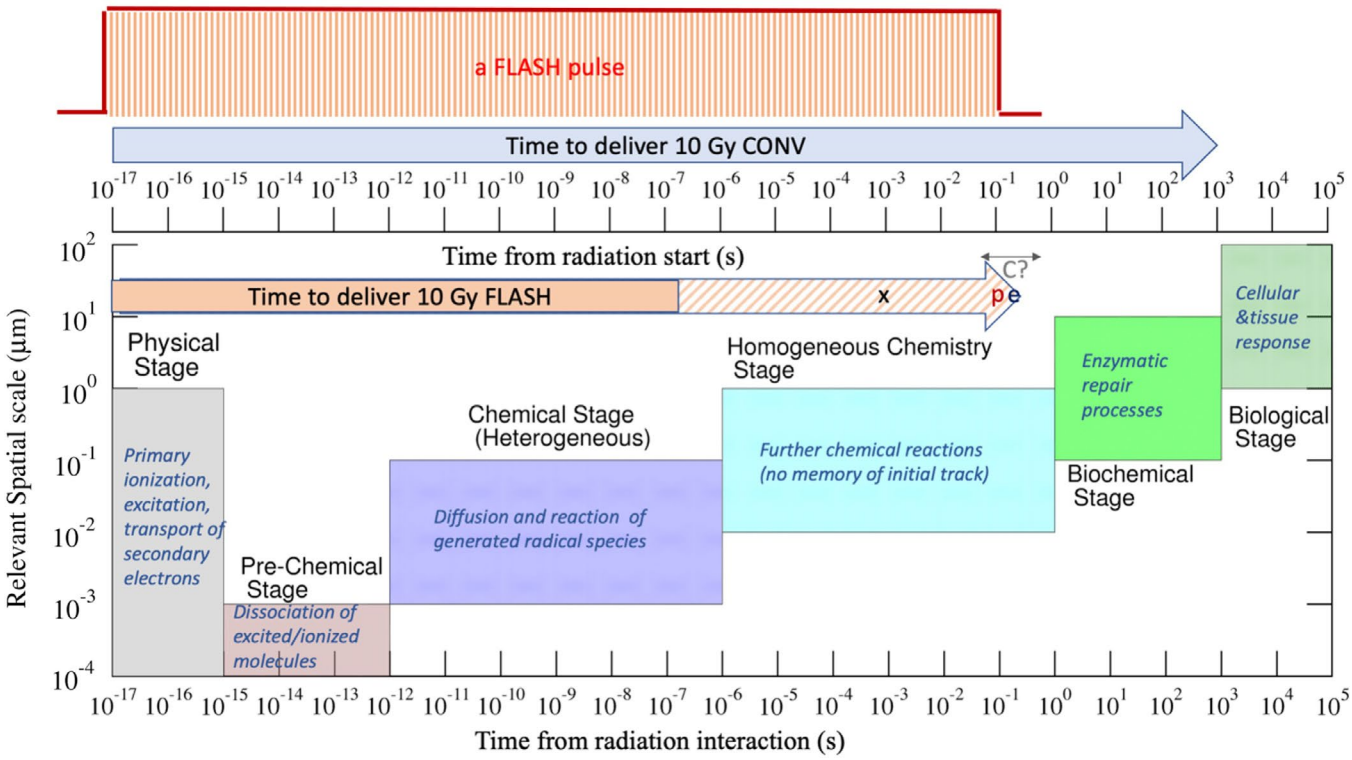

FIGURE 2 Temporal and spatial scales involved in a typical ion beam radiation damage process as compared to the length of a FLASH pulse and the T_{10}, the time needed to deliver 10 Gy in both irradiation modalities. The spatial scale, orientative for biological processes, is intended as a distance from the primary event of energy deposition, as also considered in similar schemes.[88] The shaded area of the FLASH arrow represents the range where the effect was observed preclinically (according to Ref. [7]) and the particle symbols correspond to the limit value for positive result found for each modality (x, p, e). The tentative line on the C represents the range of T_{10} values achievable, depending on the irradiated volume, according to the technique described in the next Section 3

In Figure 3, it is shown the tridimensional OER profile as a function of pO_2 and LET, and the connected quantity $\overline{OER}$ (see Appendix A1 for details) computed with the parametrization proposed by Scifoni et al.[20] From the cuts of the OER surface at increasing LET it is clearly visible that the slope of the sensitivity decrease becomes more shallow at high LET. From the plot of the $dOER/dpO_2$, it is evident that, even at the LET values typically encountered in the normal tissues, the same depletion of a given amount of oxygen, would have a sensibly smaller effect as compared to conventional—or asymptotically low LET - radiation. The $\overline{OER}$ profile across the full depth of a C-ion spread-out Bragg peak (SOBP) is shown in the same figure, for both Scifoni[20] and Wenzl–Wilkens[57] models, and compared to experimental in vitro data collected in complete anoxia.[20] While the first model[20] has been derived from in vitro data, the second one[57] was based on in vivo data. Finally, in the upper left panel, it is shown instead, the second issue mentioned above: the impact of a denser track in reducing the probability for the generated radicals to meet an oxygen molecule and react, before recombining between each other, and, as a consequence, their reduced probability to deplete oxygen.

2.3 | Impact on radical production/recombination

According to the work of Labarbe,[45] the peroxide/hydroperoxide radical recombination could have an important role in the radioprotective effective FLASH irradiation.

As we have previously demonstrated,[37] increasing LET correlates with smaller production rate of peroxide radicals because of the enhanced intratrack recombination. A similar argument was proposed by Wilson et al.[30] This is visible in the snapshots of the evolution of the chemical track for a carbon ion of 10 MeV/u, from the start to the end of the chemical stage, showing reactants and product from the initial radical conversion (Figure 4). The latter is a simplified picture, since it should be considered that in a real biological environment, different from pure water, the recombination of e^-_{aq} and $H^\bullet$ will occur more rapidly with organic radicals dispersed in the medium. In Figure 4, we also show the overall G-value of the peroxide radicals,[37] where $O_2^{\bullet -}$ and $HO_2^\bullet$ values have been summed in order not to be affected by pH and redox balances. Remarkably, it is visible that the LET effect in the radical yields

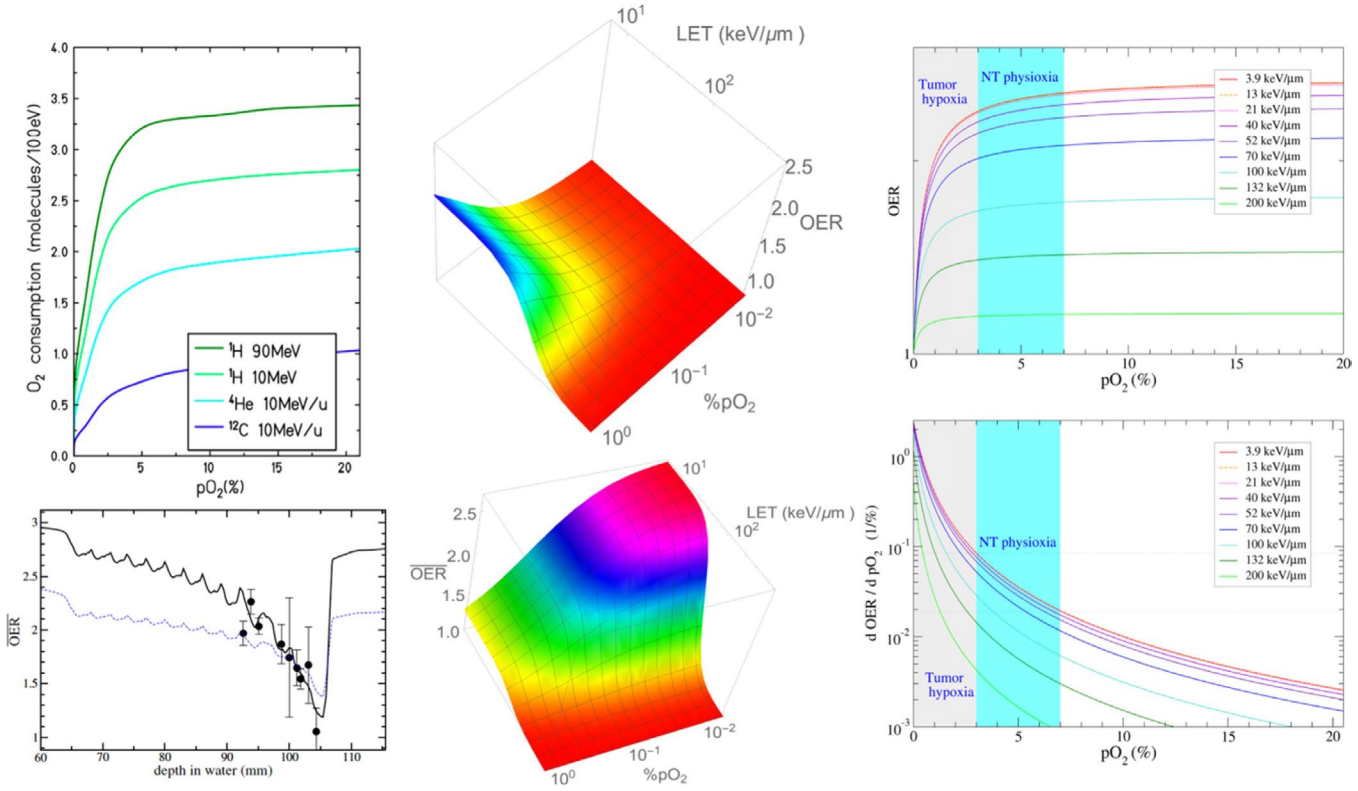

FIGURE 3 LET and oxygenation interplay: In the central panels, OER and $\overline{\text{OER}}$ profiles as a function of LET and pO_2 (modified and extended from Ref. [53]), on the right panels, focus on several OER surface cuts at fixed LET and corresponding derivative, as compared to typical regions of physioxia and tumor hypoxia. Upper left panel, calculation of O_2 consumption for different particles and LET (from Ref. [37]). Lower left panel, depth dose profile of $\overline{\text{OER}}$, across a Carbon SOBP, computed with TRiP-OER and two different OER models (blue, optimized for in vivo, black for in vitro, and compared to in vitro measurements—from Ref. [20])

(lower left panel) is much larger as compared to the pure radiosensitivity (OER) based one, shown above (Figure 3), since the surface starts to bend to lower values at much lower LET values, has a much less steep gradient of change, and thus the impact of LET increase starts at much lower values, having a dramatic impact in suppressing the radical yield already at 52 keV/μm.

2.4 | Intertrack effects

The intertrack recombination for positively charged particle beams is largely considered insignificant in determining, radiation chemical driven biological consequences of radiation exposure. For instance, the simulations of Kreipl et al.[58,59] with the PARTRAC code demonstrated that even at extremely high dose rates that may be reached by laser-driven accelerated beams, intertrack effects would be negligible at reasonable dose values. A recent work by Ramos et al.[60] based on TOPAS-nBio suggests that the intertrack for proton beams in the FLASH regime becomes relevant at low LET (<2 keV/μm) only. For this reason, it is expected that high-LET ion intertrack recombination will be detrimental for recombination and the potential effectiveness of a FLASH effect would anti-correlate with the LET increase.

A simple estimation in the typical LET values of carbon beams where track superimposition could play any role, can be done by computing the track profiles with an amorphous track model (the LEM III basic adopted formalism as detailed in Ref. [61]), and comparing different portions of that profiles, with the corresponding average distance of tracks delivered within the time needed for completing a chemical stage (r_{chem} = 1 μs, Figure 2), that is, the relevant time where interaction could occur in the heterogeneous stage. The latter average distance $\overline{d}$ is easily obtainable from the corresponding fluence F, depending on the specific dose rate $\dot{D}$ scaled for the latter timeframe $\left(\overline{d} = 1/\sqrt{F\left(\dot{D}\tau_{\text{chem}}\right)}\right)$.

In Figure 5, it is shown how, at different dose rates typically adopted in FLASH experiments, the corresponding intertrack distance between the particles delivered within a chemical stage, compares to the track size, in particular with its maximum extension, r_{max}, calculated using the Kiefer parametrization,[62] or with

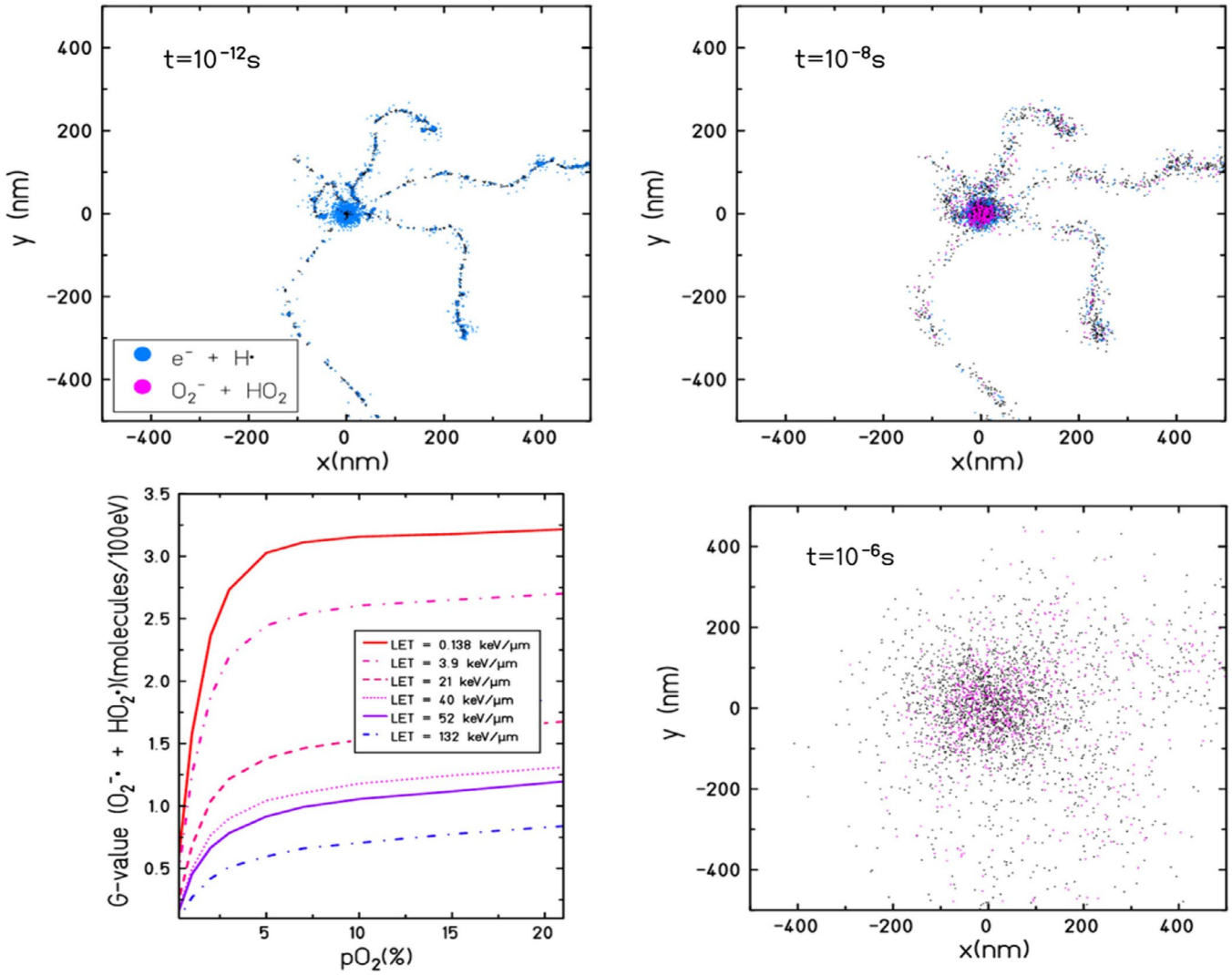

FIGURE 4 Three snapshots (panels in clockwise order) of temporal evolution within the chemical stage of a 10 MeV ^{12}C ion induced reactions from solvated electrons and H radicals toward products peroxide radicals ($O_2^{\bullet -}$ and $HO_2^{\bullet}$). The lower left panel show of overall yield of peroxide products as a function of LET and pO_2 (adapted from Ref. [37])

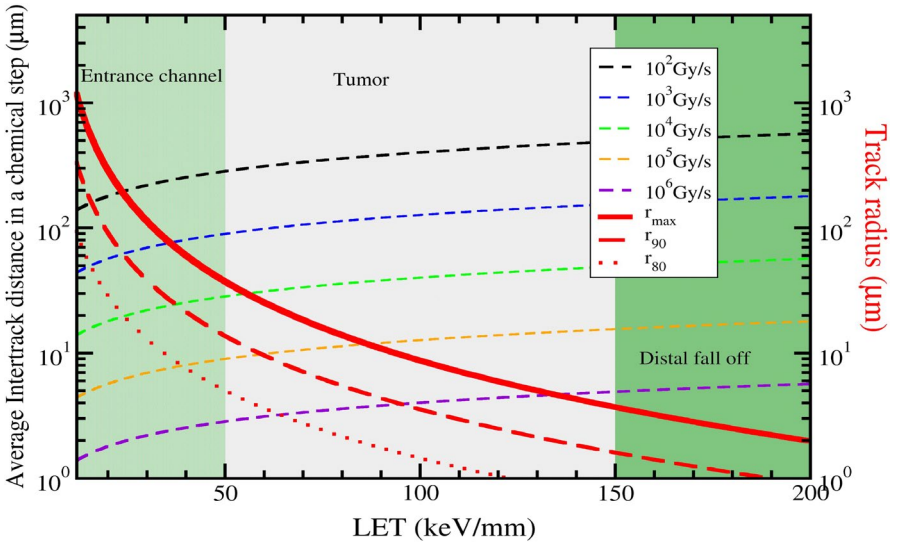

FIGURE 5 Average distance between tracks of ^{12}C ions impinging on a target within a timestep equivalent to a full chemical stage (1 μs), for different LET and intra-pulse dose rates, typically used in FLASH experiments with UHDR, as compared to the maximum extension (r_{max}) of the carbon track at the same LET, as well as to radii enclosing, respectively, 90% and 80% of the dose delivered by that track, according to an amorphous track model description

distances corresponding to 80% and 90% of the total dose delivered by that particle (see Appendix A2 for details). Considering the dose rates presently achievable with carbon (~10^2 Gy/s,) and the LET dependence, a significant effect of track overlapping can be excluded, and considering the tracks as independent entities returns a good approximation.

2.5 | LET-dependent dose modifying factors?

The high flexibility of particle beam scanning has been demonstrated for biologically driven planning with multiple fields (bio-IMPT).[63] The main challenge is the explicit consideration of different types of beam contributions, mainly described by the particle-energy spectra, and their combination. Beyond the RBE-based optimization, other types of dose modifying factors have been included in the optimization. This is for example the case of the OER in the kill painting approach,[54] or in the similar LET painting approach.[64] Biologically optimized treatment planning for UHDR will require the inclusion of a dose-modifying factor (DMF) dependent on many variables:

$$\mathrm{DMF}^{\mathrm{NT}} = \left.\frac{D_{\mathrm{CONV}}}{D_{\mathrm{FLASH}}}\right|_{\text{same effect in NT}} = \mathrm{DMF}\left(D, \dot{D}_{\mathrm{p}}, \left\langle \dot{D} \right\rangle, \mathrm{pO}_2, \mathrm{LET}, \alpha/\beta, \ldots.\right),$$

where the $\dot{D}_{\mathrm{p}}$ and $\left\langle \dot{D} \right\rangle$ are the intrapulse and overall average dose rates, respectively. These quantities play a role in the biological occurrence of the FLASH effect.[7] Should the tumor tissue also elicit a specific FLASH effect,[21] a similar tumor factor $\mathrm{DMF}^{\mathrm{T}}$ should be considered as well. Moreover, particles of different characteristics (velocity, charge) in the therapeutic beam have different effects. Hence, as for other modifiers, a dose-averaged LET dependence may not be sufficient, but rather a true mixed field averaging, a kind of "mixed FLASH field," should be necessarily computed, in order to take into account correctly the different contributions to the observed effect. This will represent an extension of the beam mixing method developed for RBE[65] and already applied to OER[66] calculation. Clearly, the definition of the dose rate is critical, and a specific definition on a voxel-by-voxel basis (e.g., the enhanced local dose rate for pencil beam scanning or the "dose-averaged dose rate" [DADR], see Section 3) should capture the biological effect dependence more directly, or possibly in combination with another microscopic parameter.

Overall, the FLASH treatment planning likely will be described by a DMF-weighted dose on a voxel-by-voxel base, and a fully biologically optimized approach.

3 | IMPLEMENTATION OF FLASH DOSE RATES AT C-ION SYNCHROTRONS

At the present time, ion-beams for carbon therapy can only be provided by synchrotron accelerators, because an energy maximum of 420 MeV/u is required to cover all relevant tumor entities with a water equivalent depth of up to 30 cm. The advantage of a synchrotron compared to the cyclotron is that the synchrotron can extract variable energies and does not require a passive degrader section, which results in high beam losses of 80%–99%. However, in contrast to the cyclotron, a synchrotron cannot continuously provide the beam. The beam is accelerated in cycles. Each cycle consists of a phase for loading the synchrotron, a phase for ramping-up the magnets and accelerating the beam and finally the extraction phase (spill). All synchrotrons used in carbon beam therapy have a cycle length of at least 1–2 s and use a "slow" beam extraction method[67] that typically lasts in the order of 0.1–10 s. As a consequence of these boundary conditions, for FLASH, the complete irradiation has to take place within a single synchrotron cycle. Otherwise, the required UHDR for FLASH of at least 40 Gy/s cannot be realized. If the irradiation extends over several synchrotron cycles and thus lasts longer than one second, FLASH conditions (UHDR) would be clearly not fulfilled.

Most of the synchrotrons for carbon-ion therapy can extract the full synchrotron filling in a short time of 100–200 ms using the slow extraction mode. Figure 6 shows a short spill (for FLASH tests) from the clinical synchrotron of the Heidelberg ion-beam therapy center (HIT).[68] The strong fluctuation (ripple) of the beam current, which is typical for all clinical synchrotron accelerators at slow extraction, can clearly be seen.

It should be noted that the fast extraction method by a kicker system with an extraction time of a few µs is not suitable for ion-beam therapy, because in that case a scanning process would not be possible and dosimetry would be too inaccurate. It is also worth noting that different "slow" extraction methods exist, like quadruple-resonance extraction,[67] the betatron core extraction,[69] and the RF-KO extraction.[68,70] In recent years a consensus has emerged that the RF-KO method is optimal for radiotherapy because the extraction intensity (particle rate) can be optimally modulated and controlled and hence allows an optimum scanning speed[67] and would, therefore, be the best option for FLASH irradiation with synchrotrons.

3.1 | Beam intensity of synchrotrons for carbon beams

As mentioned above, the main challenge for clinical FLASH irradiation with synchrotrons is the application

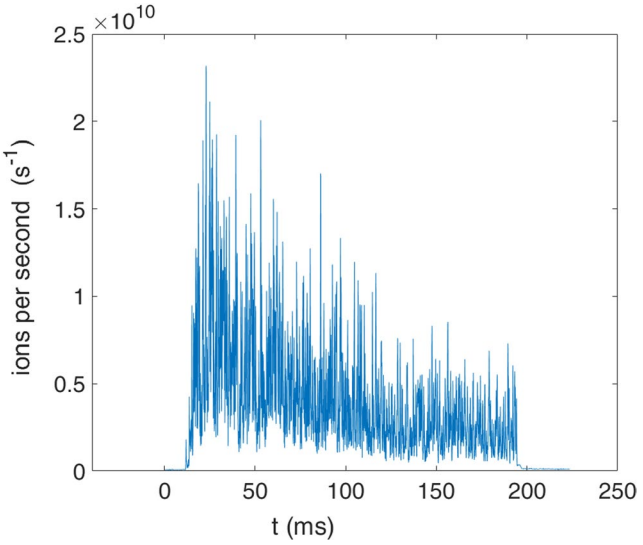

FIGURE 6 Short synchrotron spill (in slow extraction mode using the RF-KO method) recorded at the synchrotron of the Heidelberg ion-beam therapy facility (HIT) for a 280 MeV/u ^{12}C beam. The signal is recorded from the beam monitor of the scanner control system

of the complete treatment plan (for one treatment field) within one spill. In a recent work,[13] different accelerator types were assessed for proton FLASH irradiation. Similar as discussed by Jolly et al.[13] for proton synchrotrons, synchrotrons providing carbon beams face the same challenges: the amount of ions to be extracted in one synchrotron cycle (spill) is limited through space-charge effects in the ring and the injector system. This is, in particular, relevant for the compact clinical synchrotrons. The ion beam therapy facilities of Heidelberg and Marburg (HIT and MIT) are limited to <1 × 10^9 carbon ions per spill.[70,71] Recent tests for FLASH irradiations at HIT proved that spills of 5 × 10^8 carbon ions can be reliably extracted. The CNAO ion beam synchrotron in Italy—having a comparable ring diameter—can provide similar particle numbers per spill.[72] Clinical synchrotrons with a larger ring diameter like the MedAustron facility in Austria or the even bigger HIMAC[73] (NIRS) synchrotron can deliver up to 1.5 × 10^9 and 6 × 10^9 carbon ions per spill,[74,75] respectively. A large-scale research synchrotron like the one at the GSI Helmholtzzentrum can currently extract about 1 × 10^{10} carbon ions per spill. The configuration with the MUCIS source (operated with CH_4 gas)[76] and the UNILAC as an injector for the GSI SIS-18 synchrotron can presumably deliver even higher intensities for carbon ions (and protons). However, the GSI synchrotron can no longer be used for patient irradiation because the therapy pilot project[8,77] was discontinued 12 years ago. But the treatment rooms Cave-M and Cave-A of GSI are still operational. They are continuously used for research in ion-beam therapy and space-radiation research and would be ideal experimental places for basic research with FLASH irradiations in physics and radiobiology. This is in particular interesting because very high spill intensities (typ. 10^{10} carbon ions per spill) could be delivered there.

Under these preconditions, the following three important questions arise for the FLASH irradiation with carbon ions and will be discussed in the following paragraphs:

1. How can conformal irradiation of a tumor volume be achieved within a single spill of <200 ms?
2. Which amount of carbon ions must be extracted in one spill to irradiate realistic tumor sizes?
3. What role does raster scanning play for the (local) dose rate?

3.2 | Possible beam application techniques for carbon FLASH

This section discusses different techniques for tumor-conformal FLASH irradiation with carbon ions.

As shown above, the complete irradiation of the field must be carried out within one synchrotron cycle. Therefore, the standard multi-layer raster scanning method[78] cannot be applied for FLASH. This is a strong restriction since this method is the most common beam application technique for conformal irradiation and is used at most facilities like the HIT, MIT, CNAO, MedAustron, and NIRS.

3.2.1 | Multiple energy-extraction within one synchrotron cycle

However, some years ago, a synchrotron operation method became available that allows the extraction of multiple energies within one synchrotron cycle.[75] In combination with a fast raster scanning, as realized at the NIRS facility,[79] the multiple energy extraction could be a solution for FLASH. Nevertheless, all energy layers have to be scanned in less than 200 ms for FLASH and the switching time between energy steps lasts typically 100 ms at HIMAC,[75] which is currently the most advanced facility concerning scanning speed. Therefore, only extremely small tumors with maximum of 1–3 layers could be treated by this method. Future improvements for scanning parameters and in particular for the energy switching time could turn multi-energy extraction in combination with fast scanning into an interesting option for FLASH. But, at present, due to the tumor size limitation, it seems not to be an applicable option. It should be noted in that context, that modern 3D-printed ripple filters[80] allow depth steps up to 6 mm between the energy layers, which in turn could further enlarge the possible tumor size.

3.2.2 | Passive beam application by scattering

Another option is the passive beam application technique, which was developed at the Lawrence Berkeley Laboratory the first time for carbon ion therapy and further improved at the HIMAC facility.[81] In principle, if the passive scattering system is used as a fully static device and layer stacking[82] is not used (because the mechanical movement of the range shifter would be too slow), passive FLASH irradiation is conceivable for small to medium-sized tumors, if the accelerator provides sufficient intensity. Diffenderfer et al. recently presented a passive setup[83] for a cyclotron proton beam that could provide FLASH conditions (typ. 80 Gy/s @ 15–20 Gy) at target volumes of a few cm^3 for murine studies.

Nevertheless, the static passive system would not achieve the same conformity as a raster scanning system. Additionally, a passive system requires a significantly higher beam current than an active raster scanning system (for the same tumor volume), because the beam transmission losses in the scattering system and the collimator would be higher than 50%.[13] This is in general critical, because the beam intensity is the major issue for FLASH beam application.

3.2.3 | Fast beam application with 3D range modulators

Finally, a relatively new beam application method is presented here, which has good potential to enable FLASH irradiations: The so-called patient-specific 3D range modulator (3DRM)[23,84] is a passive device with many pyramid-shaped fine structures (pins), whose shape and height are optimized and adjusted to the form of an individual patient's tumor. By irradiating the 3DRM with only one energy, homogeneous dose distributions can be achieved with a significant reduction in the treatment time. The delivered dose shows conformity that is comparable to the standard 3D raster scanning method with multiple layers. The 3DRMs are manufactured with high-quality 3D rapid prototyping techniques. Figure 7 (upper part) shows the principle for dose shaping with a 3DRM for the case of a spherical volume. It should be noted that raster scanning is mandatory for beam application with 3DRMs. The fluences used to irradiate the modulator are not homogeneous, as shown in Figure 7.

In principle, every treatment plan for standard raster scanning can be converted into a 3DRM scanning plan (one energy) and in a design for a 3DRM, respectively. However, the range in-depth (in beams-eye-view) at a certain tumor position must not be too large; otherwise, the filigree pin structures cannot be manufactured. Currently, pin sizes up to 60 mm (≈70 mm H_2O) were tested, however, pin sizes up to 100 mm are technically conceivable.

Figure 7 (lower part, left) shows the design of a 3DRM that was planned for non-small-cell lung cancer (NSCLC) with a size of about 25 cm^3, the corresponding target volume, and dose distribution in a transversal CT plane is shown at the right side of Figure 7. The most relevant parameters of this plan are shown in Table 2 in the next section together with some other plans, in order to assess the feasibility of 3DRMs for different tumors and sizes.

It is obvious that 3DRMs have good prerequisites for conformal FLASH irradiations of small and small-to-medium-sized tumors due to the single-energy mode. It should be also noted that 3DRMs are being discussed intensively for proton FLASH. In the work of Jolly et al.[13] it was stated that 3D-printed patient-specific range modulators present the most likely route to clinical delivery for FLASH irradiation.

3.2.4 | Transmission fields

Finally, another option for a FLASH beam application should be mentioned, which is not discussed further here, namely simple irradiation with maximum accelerator energy and raster scanning over the lateral extension of the tumor. This method called “transmission fields”[85] however, cannot yield a 3D-conformal dose distribution with one beam direction (field), or requires several fields, which in turn cannot be applied in a short time (of few hundreds of milliseconds) and is questionable whether FLASH conditions are fulfilled. Nevertheless, this method will be applied for the first clinical FLASH trial[86] with protons for bone metastasis at the Cincinnati Children's Hospital.

3.3 | Particle numbers per spill needed for the irradiation of various treatment plans and other critical parameters for FLASH

A series of treatment plans for carbon ions were created with the treatment planning program TRiP (Version TRiP98).[25] All plans were optimized for a homogenous biologically equivalent dose in the target volume. The LEM1[26] model with an α/β ratio of 2 was applied, which is still a standard for the clinical treatment at HIT and MIT. The goal of this simple study is to assess the number of ions needed to irradiate the target volume and to estimate the dynamic requirements (e.g., scanning speed) for the scanning process.

The first series of plans (see Table 1) was calculated for a spherical volume with a 25 mm radius (depth = 80–130 mm) in a water phantom. Different RBE-weighted doses ranging from 1 to 14 Gy were applied in order to assess the variation of the RBE values, which has a direct impact on the required

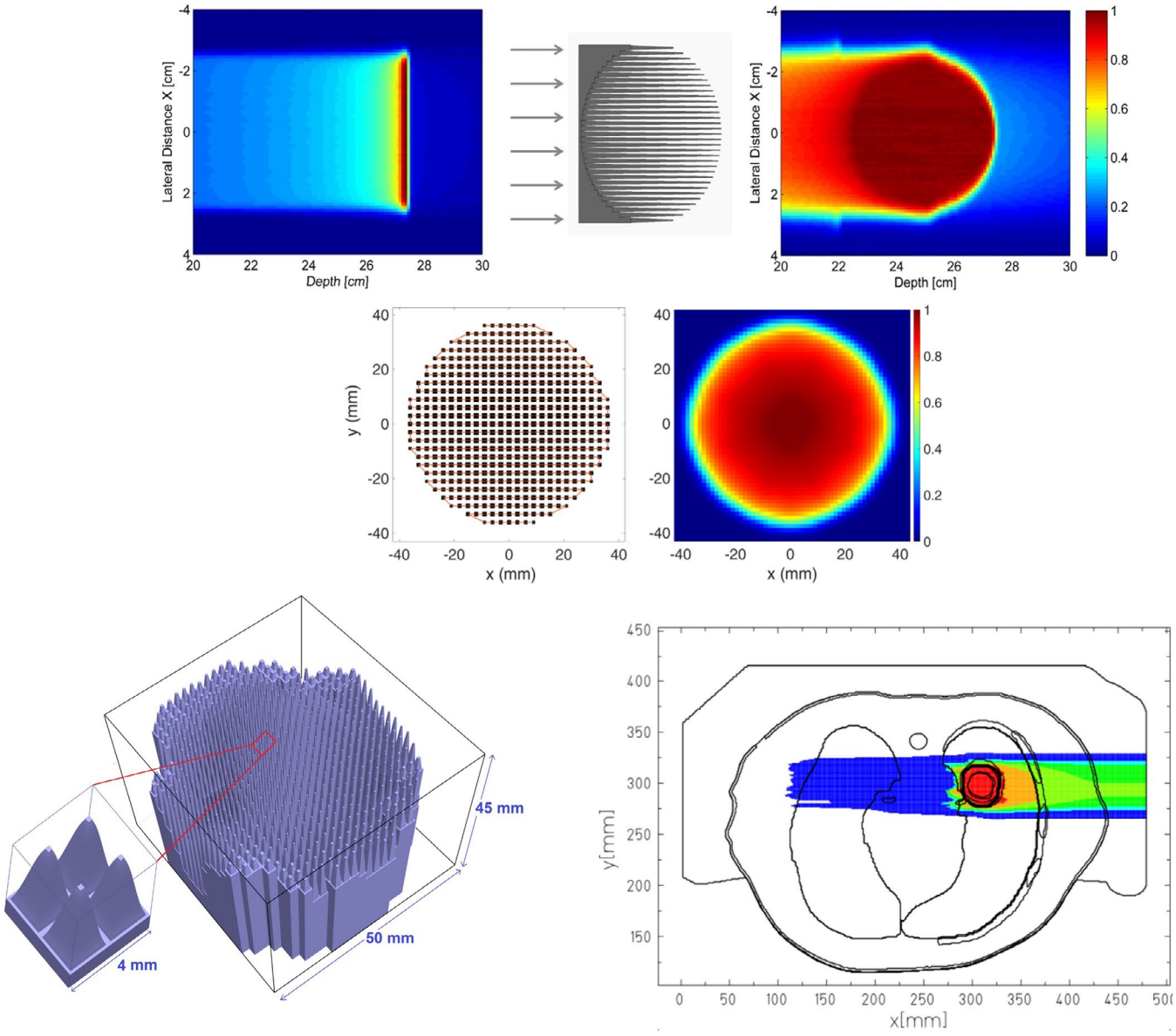

FIGURE 7 Examples of 3D range modulators: Upper figure: principle of the dose application with a 3DRM for a spherical target volume (r = 25 mm) with a single-energy beam of 400 MeV/u ^{12}C. The scatter plot in the mid shows the raster scanning pattern and the fluence map for the irradiation of the sphere. Lower left figure: Design of a 3DRM for the FLASH irradiation of small lung carcinoma (25 cm^3, see Table 2) with a 240 MeV/u ^{12}C beam. The zoom shows four of the inner pins of the modulator with a height of approx. 50 mm and a lateral size of 2 × 2 mm^2 per pin; note: the zoomed figure is not isometric, the lateral direction is enlarged for better visualization of the pin shape. Lower right figure: The corresponding dose field and the target volume in a transverse plane of the treatment plan

number of carbon ions. An RBE-weighted dose of 14 Gy corresponds roughly to 10 Gy physical dose, which is a representative dose value for FLASH irradiation. Table 1 shows the biological and the physical dose in the center of the target volume and at the entrance channel at a depth of 1 cm H_2O. It should be noted that the physical dose in the target volume is not homogenous.[26] The RBE values (ratio between biol. and phys. dose) are given as well. It can be observed, that for the assumed biological model (LEM-I, α/β = 2 Gy) the RBE value in the center of the target volume decreases from 5.4 to 1.4, when increasing the RBE-weighted dose 1–14 Gy. Accordingly, an increase of the RBE-weighted dose from 1 to 14 Gy requires about 50 times more carbon ions, which is an additional challenge in terms of providing enough beam intensity for FLASH. It should be also mentioned, that for this LEM-I model the ratio (see column 7 of Table 1) of RBE in the target volume to the RBE in the entrance channel—which could be considered as the radiobiological benefit of carbon ion treatment compared to proton therapy—decreased from 1.25 to a value of about 1 (no more benefit). However, this consideration is preliminary and could potentially be

TABLE 1 Comparison of the physical and biologically equivalent dose values for carbon ion treatment plans of a spherical target volume (r = 25 mm) calculated by the LEM-I model (α/β = 2 Gy) for RBE-weighted doses from 1 to 14 Gy

Target dose biol. equ. **(GyE)**	**Target dose** phys. **(center) (Gy)**	**RBE**	**Entrance dose** biol. equ. **(GyE (RBE))**	**Entrance dose** phys. **(Gy)**	**RBE**	**RBE-target/ RBE-entrance**	**Total number of particles for the field**
1	0.19	5.39	0.55	0.13	4.31	1.25	1.04E + 08
2	0.49	4.10	1.19	0.34	3.52	1.17	2.75E + 08
4	1.41	2.84	2.52	0.98	2.58	1.10	7.99E + 08
6	2.70	2.22	3.91	1.86	2.11	1.05	1.53E + 09
8	4.29	1.87	5.32	2.93	1.82	1.03	2.43E + 09
10	6.03	1.66	6.76	4.14	1.63	1.02	3.45E + 09
12	8.04	1.49	8.20	5.46	1.50	0.99	4.57E + 09
14	10.08	1.39	9.65	6.83	1.41	0.98	5.76E + 09

Note: The physical dose is given at the center of the CTV. The dose at the entrance channel (normal tissue) is given in 1 cm depth.

over-compensated by a FLASH effect, which can be proved only by pre-clinical experiments.

The second series of treatment plans (see Table 2) consists of plans for five different spherical volumes in water and six further treatment plans based on real patient CTs. The chordoma plans correspond to real carbon ion treatments in the GSI therapy pilot project. The lung carcinoma cases originate from contoured patient CTs (for photon IMRT). All the presented plans in Table 2 describe only one field (one beam direction) with our FLASH standard dose of 10 Gy physical dose in the center of the target. They are optimized for a homogenous biological effect (as the plans for Table 1), but are adapted for better technical comparison to a physical dose of exactly 10 Gy in the center.

The entries given in the first 6 columns of Table 2 are valid for both, standard multi-layer raster scanning and irradiation with a 3D range modulator. The further columns (7–16) are specific for the irradiation with the 3DRM. As mentioned above, the scanning plans for the 3DRMs are based on dose optimization with TRiP. In a first step, TRiP calculates the treatment plan for the standard raster scanning method, afterward the weights of all beam spots of the TRiP plan are converted for the application with a 3DRM into a single-energy scanning plan and into the shape (CAD file) of the 3DRM.

Most relevant for the feasibility of FLASH is the number of carbon ions needed for the different plans, which is shown in column 6 of Table 2. The number of ions increases almost linear with the target volume, a bit less for the larger volumes. In this table, some cells are highlighted in yellow or red. This means that the parameter in the table are critical or impossible, respectively, if the performance parameters for the accelerator and scanning system from GSI (Cave-M experimental room) are assumed. This means specifically a maximum of 1×10^{10} carbons per spill (see above) and a scanning speed in the x-direction of 28.7 mm/ms for 400 MeV/u carbons (and correspondingly higher for smaller energies). Of the facilities discussed in Section 3.1, the GSI parameters are in the upper level (however, HIMAC yields three times higher scanning speed). But also for other facilities and/or target volumes, Table 2 gives a good impression, of a FLASH irradiation is feasible or not, when assuming the specific performance parameters and scaling the values of the given table.

Column 3 shows the maximum depth range of all individual beam spot positions in the plan, which corresponds to the maximum pin height of the 3DRM (which should not exceed 8 mm of plastic ≈ 10 mm H_2O equivalent). The lateral step size and the number of the beam spots for the single-energy 3DRM plans are given in columns 8 and 9. For the virtual processing of the plans an extraction time of ca. 200 ms (186 ms) is assumed in all cases. This short extraction time could be realized at HIT and at GSI in many experiments. The corresponding (global) dose rate is given in column 10. This value is simply defined by the physical dose (center of the target) divided through the total irradiation time (start-stop of the beam extraction). Column 9 shows the total moving time t_{jump} relative to the total irradiation time. This "jump time" is defined as the time that the scanner needs to move between the beam spots and depends on the length of the scanning path (number of beam spots), the scanning speed, and beam rigidity. A relative jump time higher than 15% can be considered as critical for an accurate (homogeneous) dose distribution, higher than 30% cannot be accepted (note: rescanning cannot be applied for FLASH). An additional proton treatment plan is also given for the medium lung CA case. This serves in particular for the assessment of the local dose rate (see next section).

In summary, if we assume exemplarily GSI performance parameters, it can be stated, that tumor volumes larger than 200 cm^3 cannot be treated with FLASH and volumes between 150 and 200 cm^3 are borderline. However, small to medium-sized tumors up to 150 cm^3 should be feasible for FLASH irradiation with a 3DRM, if the facility can provide performance parameters comparable to GSI. GSI is an ideal facility for pre-clinical

TABLE 2 Relevant parameters of a series of different treatment plans for FLASH irradiation using raster scanning and 3DRMs (single energy irradiation) for carbon ion beams (and protons in one case)

	Vol. (CTV)	Max. depth range	E_{max}	Dose @mid of target		No. of beam spots	Step size	Irrad. time	Scan moving time	Global dose rate	Scan boost factor for local dose rate (phys. dose)				
				phys. | biol.				t_{global}	t_{jump}						
Case	(cm^3)	(mm H_2O)	(MeV/u)	(Gy | Gy(RBE))	No. of ions	(mm)	(mm)	(ms)	(%)	(Gy s^{-1})	DADR	98%	95%	90%	80%
Sphere r = 15 d = 50	14	30	174	10.0 | 15.1	1.6E + 09	97	3	186	3.2	54	12.7	2.1	2.4	2.9	3.2
Sphere r = 20 d = 75	35	31	215	10.0 | 14.7	3.4E + 09	177	3	186	6.7	54	27.2	3.2	3.3	4.3	4.5
Sphere r = 25 d = 75	67	50	222	10.0 | 14.4	5.5E + 09	261	3	186	10.4	54	41.3	3.9	4.0	5.2	5.5
Sphere r = 35 d = 125	182	51	291	10.0 | 14.3	1.3E + 10	489	3	186	25.6	54	71.7	4.1	5.5	7.0	7.4
Sphere r = 50 d = 150	526	101	331	10.0 | 13.7	3.0E + 10	941	3	186	47.1	54	152.2	5.8	7.8	9.9	10.9
Lung CA small	25	41	184	10.0 | 14.1	3.8E + 09	453	2	186	12.2	54	19.0	2.5	2.9	3.2	3.9
Lung CA medium	59	63	225	10.1 | 14.1	7.1E + 09	893	2	186	23.3	55	19.7	3.6	4.1	4.8	5.5
Lung CA for prot.	59	64	128	10.0 | 10.0	1.1E + 11	1110	3	186	9.3	55	2.9	1.4	1.6	1.7	1.9
Chordoma small	43	72	314	10.0 | 14.0	5.0E + 09	235	3	186	10.7	54	9.6	2.2	2.5	2.7	3.2
Chordoma medium	231	110	391	10.0 | 14.0	1.9E + 10	559	3	186	31.1	54	33.0	3.2	3.9	4.3	5.3
Chordoma large	477	138	334	10.0 | 14.4	2.1E + 10	1083	3	186	55.0	54	43.9	5.3	6.4	7.0	8.6

Note: The plans with spherical volumes of different sizes from 14 to 526 cm^3 are optimized for a homogenous RBE-weighted dose in the CTV of about 14 Gy(RBE) and have a physical dose of 10 Gy in the center of the target. The lower rows in the table show different treatment plans based on real patient CTs and converted for the irradiation with 3DRMs. As for the spherical plans, they are also optimized for 10 Gy physical dose in the target center, which yields around 14 Gy(RBE) RBE-weighted dose. The red highlighted cells show unfeasible parameters (corresponding to the given technical assumptions), the yellow ones show borderline parameters. Explanations for the local dose rate values ('scan boost factors') are given in Section 3.4. The columns (7–16) are specific for irradiation with a 3DRM.

FLASH studies with carbon ions for radio-biological samples and animal models.

3.4 | Which role plays raster scanning for the (local) FLASH dose rate?

In the previous sections, in particular, in Table 2, the "global" dose rate was conservatively calculated as the ratio of the physical dose (i.e., in the target center) divided through the total irradiation time (start–stop of the beam extraction). However, due to the raster scanning procedure and the sharp pencil beam, the dose at a certain position in the field is applied in a much shorter time, than the total irradiation time. This is especially the case for irradiation with the 3DRM, where the whole target volume is covered by only one scan with a single energy. A representative example, Figure 8 shows the local dose rate as a function of time for two arbitrarily selected voxels in the entrance channel of the irradiation field for the medium-sized lung CA from Table 2. It can be clearly seen that the major part of the local dose (here 90%) is applied in much less than the total treatment time.

Biological volume effects with signaling over several mm in a few hundred microseconds are not conceivable. Any eventual biochemical or biological interaction (for instance by protein transport or by oxygen diffusion) would last much longer. Therefore, the partial volumes of the irradiated tissue can be considered decoupled for the short treatment time. We make the hypothesis that the tissue cannot distinguish whether a (higher) local dose rate is applied everywhere in the volume of interest at exactly the same time or at slightly different times, when the time differences are much smaller than possible biological signaling. Following this hypothesis, the above-mentioned higher local dose rate by scanning would be relevant for the FLASH effect. Possible tissue and volume effects are not affected by this hypothesis. It should be also noted that "local dose-rate" is here considered as the conservatively calculated quantity as described below.

Pursuing this argumentation further, a small systematic study for the assessment of the local dose rate for fast scanning was performed in this work. A MATLAB program was implemented, which uses as input a selected 3DRM treatment plan and the time-dependent particle rate of a spill, as shown in Figure 6, but scaled by the number of particles needed for the whole plan. The algorithm calculates for every voxel in the treatment field the time-dependent accumulated dose and dose rate $\dot{D}(\vec{r}\,,t)$ for the given treatment plan. In the next step, it searches for each voxel in the treatment field and for a certain dose fraction (e.g., 90%, 95% or 98% of the total dose in this voxel) the corresponding shortest time interval, which delivers the assumed dose fraction and thus the corresponding local dose rate $\dot{D}_{\text{local}}(\vec{r}\,)$ for this voxel. The dose rate values for every voxel and for all dose fraction values between 0% and 100% are stored and analyzed for dose-rate–volume histograms (see below).

Another independent and recent work from Folkerts[85] et al. follows a comparable concept for the analysis of proton FLASH irradiations in order to assess the local dose rates. The proposed algorithm is similar to our algorithm, but uses simple thresholds (e.g., 5% and 95% for the 90% dose fraction) to identify the time intervals for dose rate calculation. This delivers slightly underestimated dose rates, in particular for smaller dose fractions (<80%); however, for the high dose fraction (95% or 98%) both algorithms deliver almost the same values (compare Figure 9, right). It should be noted that they assumed a one-energy "transmission field"

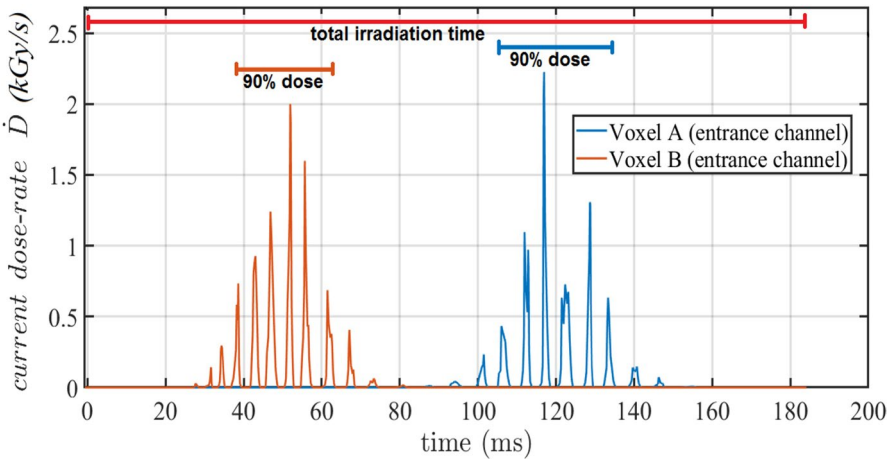

FIGURE 8 Time course of the local dose rate $\dot{D}(\vec{r}\,,t)$ in two different randomly selected voxels (A and B) in the entrance channel of the treatment fields ("Lung CA medium," see Table 2). The dose rate oscillation results from the beam wobbling. The blue and red bars indicate the smallest time interval where 90% of the total dose in the voxel (A respectively B) is applied. The broad red bar shows the total irradiation time of the field

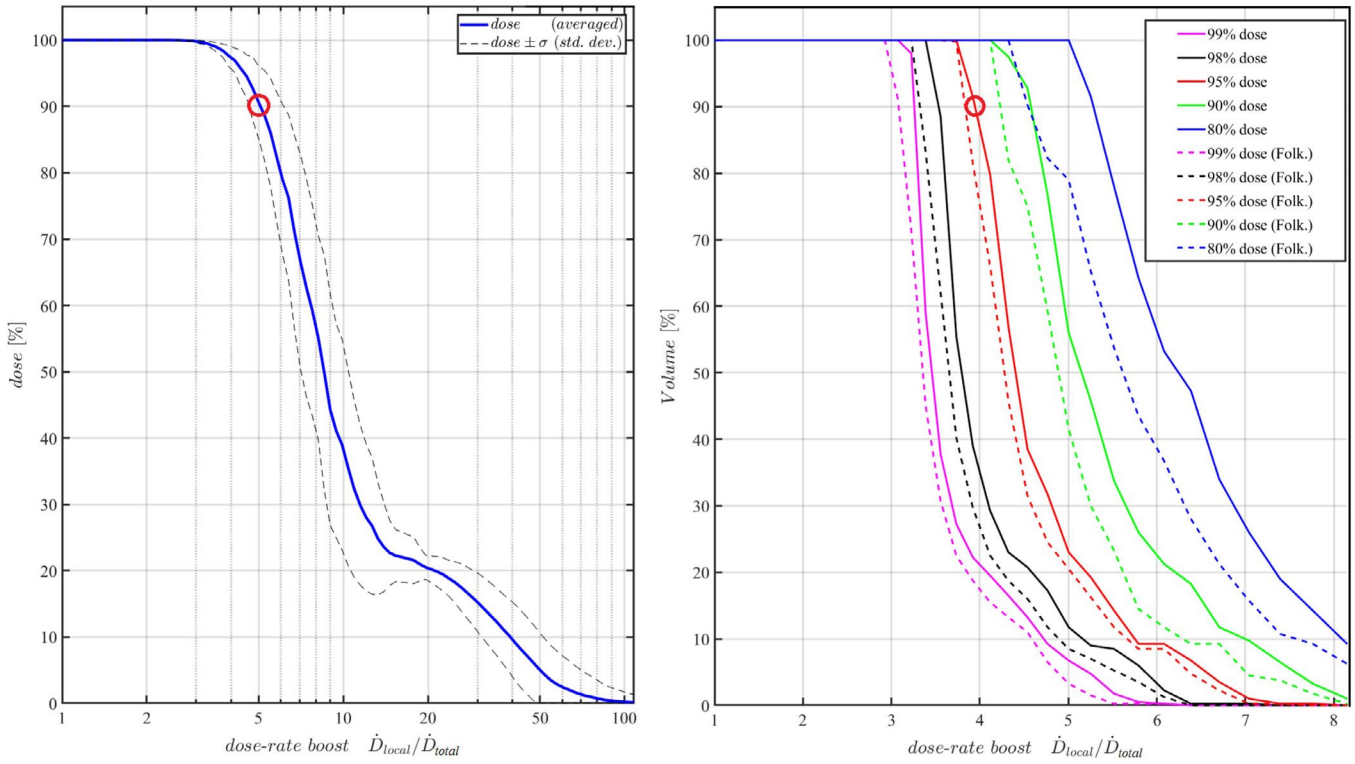

FIGURE 9 Histograms showing the enhancement of the local dose rate (boost) by the raster scanning process for a 225 MeV/u carbon FLASH irradiation plan with a 3D range modulator of medium-sized lung carcinoma (see Table 2). The dose-rate boost (*x*-axis of both graphs) indicates the local dose rate relative to the total dose rate. Left: Histogram for the fraction of the dose of a voxel (relative to the full dose in the voxel) which is applied at a certain $\dot{D}_{\text{local}}(\vec{r})/\dot{D}_{\text{total}}(\vec{r})$ value. The *y*-values are averaged over all voxels in the entrance channel; the dashed lines indicate the standard deviation of the dose averaging. Right: Histograms of the fraction of the volume in the entrance channel which is irradiated by a certain $\dot{D}_{\text{local}}(\vec{r})/\dot{D}_{\text{total}}(\vec{r})$ value. The different lines indicate the relative dose fractions (99%, 98%, 95%, 90%, and 80%) of the individual voxels for which the corresponding local data rate is applied. The dashed lines show the corresponding histogram curves for the Folkerts[84] threshold algorithm. The red circles serve for a detailed explanation of the histograms in the text

as mentioned in Section 3.2.4. Zou et al.[87] have also recently studied the limitations in volume that can be scanned under FLASH conditions.

Figure 9 shows two different dose-rate histograms for the irradiation with the 3DRM of the medium-sized lung CA of Table 2. The so-called "dose-rate boost" is defined as the ratio between the local dose rate and the total rate $\dot{D}_{\text{local}}(\vec{r})/\dot{D}_{\text{total}}(\vec{r})$ of a certain voxel, where $\dot{D}_{\text{total}}(\vec{r})$ is simply defined as the total dose of the voxel divided by the total irradiation time for the complete field. The left diagram displays the fraction of the dose which is applied at a certain dose rate value, where the dose fraction values are averaged over all voxels in the entrance channel. The dashed lines show the standard deviation ($\text{dose}_{\text{mean}} \pm \sigma$) of the averaging. It should be noted, that the dose fraction for the individual voxels (before averaging for the *y*-value of the diagram) is calculated relative to the total dose of the voxel itself (not to the global dose rate, see above). The red circle in the left diagram indicates (exemplarily) that 90% of the dose (averaged over all individual voxels) is deposited at a dose rate that is five times higher than the total dose rate of the voxels.

The right diagram of Figure 9 shows for the same data the dose-rate–volume histogram, once for the interval-search algorithm of this work (solid line) and once for the Folkerts threshold algorithm (dashed lines). The exact meaning of these histograms can be best explained exemplarily by the red circle: it indicates that 90% of the voxels in the entrance channel (treated normal tissue) are irradiated in a way that a dose fraction of 95% is irradiated by a dose rate, that is at least four times higher than the total dose rate (or in other words: at least four times shorter than the total irradiation time). It should be mentioned that the dose-rate boost factors for the entrance channel are similar to those of the target volume. Nevertheless, we only present data for the entrance channel, because this is the region where a FLASH effect is expected.

The last columns of Table 2 show the corresponding scanning boost factors $\dot{D}_{\text{local}}(\vec{r})/\dot{D}_{\text{total}}(\vec{r})$ for different dose fractions (80%, 90%, 95%, and 98%) averaged over all voxels in the entrance channel. It can be clearly seen, that the boost for large target volumes is much stronger than for small volumes. This can be simply explained by the fact that, that the ratio of the time for the

scanning of the total volume to the scanning time for a local voxel (compare Figure 8) increases with the size of the target volume (roughly $\sim \sqrt[3]{V}$).

Table 2 shows also a case for a proton plan, which has the same target geometry as the carbon ion plan for "Lung CA medium." This case is in particular interesting, because it shows that for the three times broader pencil beam—that was assumed for protons—the boost for the local dose rate is much lower. The explanation is, that more scanning lines are needed for protons to reach a certain dose fraction (e.g., 95%) than with carbon ion, because the beam is broader. This leads correspondingly to a longer local irradiation time and lower local dose rate.

Additionally, in our study, we calculated the so-called "dose-averaged dose rate" values (DADR) corresponding to the formula given by the work of Van de Water et al.[88] These values—averaged over the volume of the entrance channel—are shown in column 10 of Table 2 (relative to the global dose rate). However, these values overestimate the local rate, because the DADR concept does not reflect the time-course of the local dose rate. For example, the formula does not consider the length of the pauses between peaks of $\dot{D}(\vec{r}, t)$. This is in particular important for the irradiation by scanning, as can be seen in Figure 8. This effect also explains the strong deviations between the dose-rate boost factors for the DADR concept and the values from this work as shown in Table 2.

Finally, it raises the question: what is the benefit of the dose rate boost by scanning? In any case, the FLASH irradiation has to be applied within one spill. This means that the requirements for the accelerator are not mitigated by the dose-rate boost, because the total dose (number of ions) needed for the FLASH irradiation is independent of the dose rate. However, for some cases of medium sized target volumes (e.g., "sphere $r = 25$ $d = 125$" or "Lung CA medium" of Table 2) the extraction time could be extended, for example, by a factor of 3 and the dose rate conditions would be still fulfiled. This could mitigate the issue of too fast scanning speed and would reduce the t_{jump} to an acceptable limit (see col. 10 in Table 2).

Another important benefit of the extended extraction time would be the mitigation of the dose saturation effects in the beam monitors and dosimetry detectors.

4 | CONCLUSIONS

The perspective of using carbon ions at FLASH regimes opens several new challenges and opportunities, both on the scientific and technical level, in terms of radiobiology, dosimetry, and dose delivery. Definition of new quantities, such as specific dose rates, and their impact on radiobiological effect will be a fundamental step in this aim.

From the radiobiology point of view, the question remains whether a FLASH effect will be seen with heavy ions, as it has been shown with electrons and protons. As we detailed in the first part of this work, this is difficult to predict, for the simple reason that the mechanism of the FLASH effect is still unclear. Moreover, C-ion therapy is a peculiar mix of low- and high-LET radiation, and even most of the tumor is exposed to moderate LET values, generally lower than typical high-LET reference radiation such as α-particles.[10] However, by briefly analyzing some of the most explored potential FLASH pathways, namely, oxygen depletion, radical recombination, and intertrack effects, it appears that according to the current models for the FLASH effect, the normal tissue protection for high dose-rates observed with low-LET radiation will be partially lost using densely ionizing radiation. In fact, at high-LET, the intertrack recombination will not significantly contribute. Moreover, a possible tumor sensitization has been predicted by some models, but it remains to be demonstrated.

As for realizing with carbon ion beams the dosimetric conditions allowing UHDR exploitation comparable to the other modalities, from the technical point of view, the use of synchrotrons for FLASH is complicated in terms of intensity and time structure. FLASH regimes with UHDR in full multi-energy-layer pencil-beam scanning are essentially not possible with current heavy ion synchrotrons. In this paper, we have used the high-intensity SIS18 synchrotron at the GSI Helmholtz Center for reference. Using 3D range modulators, we have shown that tumors <150 cm^3 can be irradiated with C-ions in UHDR regimes. Additionally, the local dose rate for pencil beam scanning—depending on the target volume and sharpness of the pencil beam—is enhanced even more by a factor of typically 2–10.

Overall, we can summarize a number of open questions that will need to be addressed specifically in this new fascinating field of Carbon-FLASH (beside the pending questions on the FLASH effect in general):

1. Can a FLASH protective effect be confirmed in normal tissue with Carbon ions?
2. Can a FLASH sensitizing effect be confirmed on the tumor with Carbon ions?
3. Which are the limits in LET for both protective/sensitizing effects?
4. Are these thresholds binary values or is there a LET-dependent DMF?
5. Which is the relevant dose-rate definition for scanning that may have an impact on the preservation of the effect? Can we optimize this by scanning patterns?
6. Is there an impact on applying multiple fields or fractionation schemes for FLASH?

If FLASH leads to normal tissue sparing, it may further improve C-ion therapy and pave the way to the use

of heavier ions in therapy. Moreover, the verification of a FLASH effect in such conditions may contribute to rule out several mechanisms which are believed to play a role also for low LET radiation. If no effect is observed, it will clarify the mechanism of the FLASH effect as yet observed with light-charged particles. Either way, experimental results are eagerly awaited and will shed light on this fascinating but yet unclear topic.

In this connection, among the several international initiatives presently dedicated to different aspects of FLASH, a collaboration of research teams from GSI, HIT and DKFZ in Heidelberg started in 2019 to conduct various experiments for FLASH with carbon ions. The research program includes in vitro tests for clonogenic cell survival and residual γH2AX foci analysis at different oxygenation levels, mouse experiments, radiation-chemical and dosimetry tests at HIT, and GSI. These experiments will hopefully provide an answer to the main questions summarized above.

ACKNOWLEDGMENTS

The work on FLASH in our laboratory is part of the R&D project experiment SBio08_Weber at the beamline SIS18 in the frame of FAIR Phase-0 supported by the GSI Helmholtzzentrum für Schwerionenforschung in Darmstadt (Germany). We thank the ion-beam FLASH cooperation between GSI, HIT-Heidelberg, and DKFZ for strong motivation and the ongoing research activities in this field. ES acknowledges support from the INFN-CSNV Call MoVe-IT. We thank Daria Boscolo and Martina Fuss for their useful discussions. Open Access funding enabled and organized by Projekt DEAL.

CONFLICT OF INTEREST

The authors declare no conflict of interest.

DATA AVAILABILITY STATEMENT

The data that support the findings of this study are available from the corresponding author upon reasonable request.

REFERENCES

1. Town CD. Radiobiology. Effect of high dose rates on survival of mammalian cells. *Nature*. 1967;215(5103):847-848.
2. Berry RJ, Hall EJ, Forster DW, Storr TH, Goodman MJ. Survival of mammalian cells exposed to X rays at ultra-high dose-rates. *Br J Radiol*. 1969;42(494):102-107. https://doi.org/10.1259/0007-1285-42-494-102
3. Favaudon V, Caplier L, Monceau V, et al. Ultrahigh dose-rate FLASH irradiation increases the differential response between normal and tumor tissue in mice. *Sci Transl Med*. 2014;6(245):245ra93. https://doi.org/10.1126/scitranslmed.3008973
4. Vozenin M-C, De Fornel P, Petersson K, et al. The advantage of FLASH radiotherapy confirmed in mini-pig and cat-cancer patients. *Clin Cancer Res*. 2019;25(1):35-42. https://doi.org/10.1158/1078-0432.CCR-17-3375
5. Montay-Gruel P, Bouchet A, Jaccard M, et al. X-rays can trigger the FLASH effect: ultra-high dose-rate synchrotron light source prevents normal brain injury after whole brain irradiation in mice. *Radiother Oncol*. 2018;129:582-588. https://doi.org/10.1016/j.radonc.2018.08.016
6. Montay-Gruel P, Acharya MM, Petersson K, et al. Long-term neurocognitive benefits of FLASH radiotherapy driven by reduced reactive oxygen species. *Proc Natl Acad Sci*. 2019;116(22):10943-10951. https://doi.org/10.1073/pnas.1901777116
7. Montay-Gruel P, Acharya MM, Gonçalves Jorge P, et al. Hypofractionated FLASH-RT as an effective treatment against glioblastoma that reduces neurocognitive side effects in mice. *Clin Cancer Res*. 2021;27(3):775-784. https://doi.org/10.1158/1078-0432.CCR-20-0894
8. Schardt D, Elsässer T, Schulz-Ertner D. Heavy-ion tumor therapy: physical and radiobiological benefits. *Rev Mod Phys*. 2010;82(1):383-425. https://doi.org/10.1103/RevModPhys.82.383
9. Durante M, Paganetti H. Nuclear physics in particle therapy: a review. *Rep Prog Phys*. 2016;79:096702. https://doi.org/10.1088/0034-4885/79/9/096702
10. Tinganelli W, Durante M. Carbon ion radiobiology. *Cancers*. 2020;12(10):3022. https://doi.org/10.3390/cancers12103022
11. Durante M, Orecchia R, Loeffler JS. Charged-particle therapy in cancer: clinical uses and future perspectives. *Nat Rev Clin Oncol*. 2017;14(8):483-495. https://doi.org/10.1038/nrclinonc.2017.30
12. Castro JR. Results of heavy ion radiotherapy. *Radiat Environ Biophys*. 1995;34(1):45-48.
13. Jolly S, Owen H, Schippers M, Welsch C. Technical challenges for FLASH proton therapy. *Phys Medica*. 2020;78:71-82. https://doi.org/10.1016/j.ejmp.2020.08.005
14. Vozenin MC, Montay-Gruel P, Limoli C, Germond JF. All irradiations that are ultra-high dose rate may not be FLASH: the critical importance of beam parameter characterization and in vivo validation of the FLASH effect. *Radiat Res*. 2020;194(6):571-572. https://doi.org/10.1667/RADE-20-00141.1
15. Wilson JD, Hammond EM, Higgins GS, Petersson K. Ultra-high dose rate (FLASH) radiotherapy: silver bullet or fool's gold? *Front Oncol*. 2020;9:1563. https://doi.org/10.3389/fonc.2019.01563
16. Petersson K, Adrian G, Butterworth K, McMahon SJ. A quantitative analysis of the role of oxygen tension in FLASH radiation therapy. *Int J Radiat Oncol Biol Phys*. 2020;107(3):539-547. https://doi.org/10.1016/j.ijrobp.2020.02.634
17. Abolfath R, Grosshans D, Mohan R. Oxygen depletion in FLASH ultra-high-dose-rate radiotherapy: a molecular dynamics simulation. *Med Phys*. 2020;47(12):6551-6561. https://doi.org/10.1002/mp.14548
18. Pratx G, Kapp DS. A computational model of radiolytic oxygen depletion during FLASH irradiation and its effect on the oxygen enhancement ratio. *Phys Med Biol*. 2019;64(18):185005. https://doi.org/10.1088/1361-6560/ab3769
19. Rothwell BC, Kirkby NF, Merchant MJ, et al. Determining the parameter space for effective oxygen depletion for FLASH radiation therapy. *Phys Med Biol*. 2021;66(5):055020. https://doi.org/10.1088/1361-6560/abe2ea
20. Scifoni E, Tinganelli W, Weyrather WK, Durante M, Maier A, Krämer M. Including oxygen enhancement ratio in ion beam treatment planning: model implementation and experimental verification. *Phys Med Biol*. 2013;58(11):3871-3895. https://doi.org/10.1088/0031-9155/58/11/3871
21. Zakaria AM, Colangelo NW, Meesungnoen J, Azzam EI, Plourde M-É, Jay-Gerin J-P. Ultra-high dose-rate, pulsed (FLASH) radiotherapy with carbon ions: generation of early, transient, highly oxygenated conditions in the tumor environment. *Radiat Res*. 2020;194(6):587-593. https://doi.org/10.1667/RADE-19-00015.1
22. Colangelo NW, Azzam EI. The importance and clinical implications of FLASH ultra-high dose-rate studies for proton and

heavy ion radiotherapy. *Radiat Res*. 2019;193(1):1. https://doi.org/10.1667/RR15537.1
23. Simeonov Y, Weber U, Penchev P, et al. 3D range-modulator for scanned particle therapy: development, Monte Carlo simulations and experimental evaluation. *Phys Med Biol*. 2017;62(17):7075-7096. https://doi.org/10.1088/1361-6560/aa81f4
24. ICRU. Report 93 - prescribing, recording and reporting light ion beam therapy. *J ICRU*. 2016;16(1–2):3-4. https://doi.org/10.1093/jicru/ndy025
25. Krämer M, Jäkel O, Haberer T, Kraft G, Schardt D, Weber U. Treatment planning for heavy-ion radiotherapy: physical beam model and dose optimization. *Phys Med Biol*. 2000;45(11):3299-3317. https://doi.org/10.1088/0031-9155/45/11/313
26. Krämer M, Scholz M. Treatment planning for heavy-ion radiotherapy: calculation and optimization of biologically effective dose. *Phys Med Biol*. 2000;45(11):3319-3330. https://doi.org/10.1088/0031-9155/45/11/314
27. Elsässer T, Weyrather WK, Friedrich T, et al. Quantification of the relative biological effectiveness for ion beam radiotherapy: direct experimental comparison of proton and carbon ion beams and a novel approach for treatment planning. *Int J Rad Oncol Biol Phys*. 2010;78(4):1177-1183.
28. Tommasino F, Scifoni E, Durante M. New ions for therapy. *Int J Part Ther*. 2015;2(3):428-438. https://doi.org/10.14338/IJPT-15-00027.1
29. Krämer M, Kraft G. Calculations of heavy-ion track structure. *Radiat Environ Biophys*. 1994;33(2):91-109. https://doi.org/10.1007/BF01219334
30. Wilson P, Jones B, Yokoi T, Hill M, Vojnovic B. Revisiting the ultra-high dose rate effect: implications for charged particle radiotherapy using protons and light ions. *Br J Radiol*. 2012;85(1018):e933-e939. https://doi.org/10.1259/bjr/17827549
31. Boscolo D, Scifoni E, Durante M, Krämer M, Fuss MC. May oxygen depletion explain the FLASH effect? A chemical track structure analysis. *Radiother Oncol*. 2021;162:68-75. https://doi.org/10.1016/j.radonc.2021.06.031
32. Zhou G. Mechanisms underlying FLASH radiotherapy, a novel way to enlarge the differential responses to ionizing radiation between normal and tumor tissues. *Radiat Med Prot*. 2020;1(1):35-40. https://doi.org/10.1016/j.radmp.2020.02.002
33. Hendry J. Taking care with FLASH radiation therapy. *Int J Radiat Oncol Biol Phys*. 2020;107(2):239-242. https://doi.org/10.1016/j.ijrobp.2020.01.029
34. Spitz DR, Buettner GR, Petronek MS, et al. An integrated physico-chemical approach for explaining the differential impact of FLASH versus conventional dose rate irradiation on cancer and normal tissue responses. *Radiother Oncol*. 2019;139:23-27. https://doi.org/10.1016/j.radonc.2019.03.028
35. Koch CJ. ,Re: Differential impact of FLASH versus conventional dose rate irradiation: Spitz et al. *Radiother Oncol*. 2019;139:62-63. https://doi.org/10.1016/j.radonc.2019.07.004
36. Spitz DR, Buettner GR, Limoli CL. Response to letter regarding "An integrated physico-chemical approach for explaining the differential impact of FLASH versus conventional dose rate irradiation on cancer and normal tissue responses". *Radiother Oncol*. 2019;139:64-65. https://doi.org/10.1016/j.radonc.2019.07.009
37. Boscolo D, Krämer M, Fuss MC, Durante M, Scifoni E. Impact of target oxygenation on the chemical track evolution of ion and electron radiation. *Int J Mol Sci*. 2020;21(2):424. https://doi.org/10.3390/ijms21020424
38. Jin JY, Gu A, Wang W, Oleinick NL, Machtay M, (Spring) Kong FM. Ultra-high dose rate effect on circulating immune cells: A potential mechanism for FLASH effect? *Radiother Oncol*. 2020;149:55-62. https://doi.org/10.1016/j.radonc.2020.04.054
39. Liew H, Mein S, Dokic I, et al. Deciphering time-dependent DNA damage complexity, repair, and oxygen tension: a mechanistic model for FLASH-dose-rate radiation therapy. *Int J Radiat Oncol Biol Phys*. 2021;110:574-586. https://doi.org/10.1016/j.ijrobp.2020.12.048
40. Vozenin MC, Hendry JH, Limoli CL. Biological benefits of ultra-high dose rate FLASH radiotherapy: sleeping beauty awoken. *Clin Oncol*. 2019;31(7):407-415. https://doi.org/10.1016/j.clon.2019.04.001
41. Tabata Y. Fundamentals of radiation chemistry. *Radiat Phys Chem*. 1981;18(1–2):43-58. https://doi.org/10.1016/ 0146-5724(81)90063-7
42. Diels JC, Rudolph W. *Ultrashort Laser Pulse Phenomena*. Cambridge, MA: Academic Press; 2006. https://doi.org/10.1016/B978-0-12-215493-5.X5000-9
43. Wardman P. Radiotherapy using high-intensity pulsed radiation beams (FLASH): a radiation-chemical perspective. *Radiat Res*. 2020;194(6):607-617. https://doi.org/10.1667/RADE-19-00016
44. Hall EJ, Brenner DJ. The dose-rate effect revisited: radiobiological considerations of importance in radiotherapy. *Int J Radiat Oncol Biol Phys*. 1991;21(6):1403-1414. https://doi.org/10.1016/0360-3016(91)90314-T
45. Labarbe R, Hotoiu L, Barbier J, Favaudon V. A physicochemical model of reaction kinetics supports peroxyl radical recombination as the main determinant of the FLASH effect. *Radiother Oncol*. 2020;153:303-310. https://doi.org/10.1016/j.radonc.2020.06.001
46. Lai Y, Jia X, Chi Y. Modeling the effect of oxygen on the chemical stage of water radiolysis using GPU-based microscopic Monte Carlo simulations, with an application in FLASH radiotherapy. *Phys Med Biol*. 2021;66(2): https://doi.org/10.1088/1361-6560/abc93b
47. Michaels HB. Oxygen depletion in irradiated aqueous solutions containing electron affinic hypoxic cell radiosensitizers. *Int J Radiat Oncol Biol Phys*. 1986;12(7 PART 1):1055-1058. https://doi.org/10.1016/0360-3016(86)90224-5
48. Epp ER, Weiss H, Djordjevic B, Santomasso A. The radiosensitivity of cultured mammalian cells exposed to single high intensity pulses of electrons in various concentrations of oxygen. *Radiat Res*. 1972;52(2):324-332. https://doi.org/10.2307/3573572
49. Weiss H, Epp ER, Heslin JM, Ling CC, Santomasso A. Oxygen depletion in cells irradiated at ultra-high dose-rates and at conventional dose-rates. *Int J Radiat Biol Relat Stud Phys Chem Med*. 1974;26(1):17-29. https://doi.org/10.1080/09553007414550901
50. Adrian G, Konradsson E, Lempart M, Bäck S, Ceberg C, Petersson K. The FLASH effect depends on oxygen concentration. *Br J Radiol*. 2020;93(1106):20190702. https://doi.org/10.1259/bjr.20190702
51. Pratx G, Kapp DS. Ultra-high-dose-rate FLASH irradiation may spare hypoxic stem cell niches in normal tissues. *Int J Radiat Oncol Biol Phys*. 2019;105(1):190-192. https://doi.org/10.1016/j.ijrobp.2019.05.030
52. Meesungnoen J, Jay-Gerin JP. High-let ion radiolysis of water: oxygen production in tracks. *Radiat Res*. 2009;171(3):379-386. https://doi.org/10.1667/RR1468.1
53. Surdutovich E, Solov'yov AV. Multiscale approach to the physics of radiation damage with ions. *Eur Phys J D*. 2014;68(11):353. https://doi.org/10.1140/epjd/e2014-50004-0
54. Tinganelli W, Durante M, Hirayama R, et al. Kill-painting of hypoxic tumours in charged particle therapy. *Sci Rep*. 2015;5(1):17016. https://doi.org/10.1038/srep17016
55. Furusawa Y, Fukutsu K, Aoki M, et al. Inactivation of aerobic and hypoxic cells from three different cell lines by accelerated ^{3}He-, ^{12}C- and ^{20}Ne-Ion beams. *Radiat Res*. 2000;154:485-496.
56. Boscolo D, Krämer M, Durante M, Fuss MC, Scifoni E. TRAX-CHEM: a pre-chemical and chemical stage extension of the particle track structure code TRAX in water targets. *Chem Phys Lett*. 2018;698:11-18. https://doi.org/10.1016/j.cplett.2018.02.051

57. Wenzl T, Wilkens JJ. Modelling of the oxygen enhancement ratio for ion beam radiation therapy. *Phys Med Biol*. 2011;56(11):3251-3268. https://doi.org/10.1088/0031-9155/56/11/006
58. Kreipl MS, Friedland W, Paretzke HG. Interaction of ion tracks in spatial and temporal proximity. *Radiat Environ Biophys*. 2009;48(4):349-359. https://doi.org/10.1007/s00411-009-0234-z
59. Kreipl MS, Friedland W, Paretzke HG. Time- and space-resolved Monte Carlo study of water radiolysis for photon, electron and ion irradiation. *Radiat Environ Biophys*. 2009;48(1):11-20. https://doi.org/10.1007/s00411-008-0194-8
60. Ramos-Méndez J, Domínguez-Kondo N, Schuemann J, McNamara A, Moreno-Barbosa E, Faddegon B. LET-dependent intertrack yields in proton irradiation at ultra-high dose rates relevant for FLASH therapy. *Radiat Res*. 2020;194(4):351-362. https://doi.org/10.1667/RADE-20-00084.1
61. Elsässer T, Cunrath R, Krämer M, Scholz M. Impact of track structure calculations on biological treatment planning in ion radiotherapy. *New J Phys*. 2008;10:075005. https://doi.org/10.1088/1367-2630/10/7/075005
62. Kiefer J, Straaten H. A model of ion track structure based on classical collision dynamics (radiobiology application). *Phys Med Biol*. 1986;31(11):1201-1209. https://doi.org/10.1088/0031-9155/31/11/002
63. Krämer M, Scifoni E, Schmitz F, Sokol O, Durante M. Overview of recent advances in treatment planning for ion beam radiotherapy ⋆. *Eur Phys J D*. 2014;68(10):306.
64. Bassler N, Toftegaard J, Lühr A, et al. LET-painting increases tumour control probability in hypoxic tumours. *Acta Oncol*. 2014;53(1):25-32. https://doi.org/10.3109/0284186X.2013.832835
65. Krämer M, Scholz M. Rapid calculation of biological effects in ion radiotherapy. *Phys Med Biol*. 2006;51(8):1959-1970. https://doi.org/10.1088/0031-9155/51/8/001
66. Strigari L, Torriani F, Manganaro L, et al. Tumour control in ion beam radiotherapy with different ions in the presence of hypoxia: an oxygen enhancement ratio model based on the microdosimetric kinetic model. *Phys Med Biol*. 2018;63(6):065012. https://doi.org/10.1088/1361-6560/aa89ae
67. Singh R, Forck P, Boutachkov P, Sorge S, Welker H. Slow extraction spill characterization from micro to milli-second scale. *J Phys Conf Ser*. 2018;1067:072002. https://doi.org/10.1088/1742-6596/1067/7/072002
68. Schoemers C, Feldmeier E, Naumann J, Panse R, Peters A, Haberer T. The intensity feedback system at Heidelberg Ion-Beam Therapy Centre. *Nucl Instrum Methods Phys Res A Accel Spectrom Detect Assoc Equip*. 2015;795:92-99. https://doi.org/10.1016/j.nima.2015.05.054
69. Pullia MG, Bressi E, Falbo L, et al. Betatron core driven slow extraction at CNAO and MedAustron. In: *IPAC 2016 - Proceedings of the 7th International Particle Accelerator Conference*; 2016:1330-1333.
70. Krantz C, Fischer T, Kröck B, et al. Slow extraction techniques at the Marburg Ion-Beam Therapy Centre. *IPAC 2018 ninth Int Particle Accelerator Conf*. 2018:1084-1086. https://doi.org/10.18429/JACoW-IPAC2018-TUPAL036
71. Scheeler U, Krantz C, Sievers S, et al. Recommissioning of the Marburg Ion-Beam Therapy Centre (MIT) accelerator facility. In: *IPAC 2016 - Proceedings of the 7th International Particle Accelerator Conference*. 2016:1908-1910.
72. Rossi S. The status of CNAO. *Eur Phys J Plus*. 2011;126(8):1-39. https://doi.org/10.1140/epjp/i2011-11078-8
73. Noda K, Furukawa T, Fujimoto T, et al. Recent progress and future plans of heavy-ion cancer radiotherapy with HIMAC. *Nucl Instrum Methods Phys Res B Beam Interact Mater Atoms*. 2017;406:374-378. https://doi.org/10.1016/j.nimb.2017.04.021
74. Kurfürst C, Adler L, De Franco A, et al. Status of the MedAustron Beam Commissioning with Protons and Carbon Ions. *Int Part Accel Conf Proc*. 2018:7-10. https://doi.org/10.18429/JACoW-IPAC2018-TUPAF004
75. Mizushima K, Furukawa T, Iwata Y, et al. Performance of the HIMAC beam control system using multiple-energy synchrotron operation. *Nucl Instrum Methods Phys Res B Beam Interact Mater Atoms*. 2017;406:347-351. https://doi.org/10.1016/j.nimb.2017.03.051
76. Barth W, Adonin A, Appel S, et al. Heavy ion linac as a high current proton beam injector. *Phys Rev ST Accel Beams*. 2015;18(5):050102. https://doi.org/10.1103/PhysRevSTAB.18.050102
77. Durante M, Loeffler JS. Charged particles in radiation oncology. *Nat Rev Clin Oncol*. 2010;7(1):37-43. https://doi.org/10.1038/nrclinonc.2009.183
78. Haberer T, Becher W, Schardt D, Kraft G. Magnetic scanning system for heavy ion therapy. *Nucl Instrum Methods Phys Res A Accel Spectrom Detect Assoc Equip*. 1993;330(1–2):296-305. https://doi.org/10.1016/0168-9002(93)91335-K
79. Furukawa T, Hara Y, Mizushima K, et al. Development of NIRS pencil beam scanning system for carbon ion radiotherapy. *Nucl Instrum Methods Phys Res B Beam Interact Mater Atoms*. 2017;406:361-367. https://doi.org/10.1016/j.nimb.2016.10.029
80. Ringbæk TP, Weber U, Santiago A, et al. Dosimetric comparisons of carbon ion treatment plans for 1D and 2D ripple filters with variable thicknesses. *Phys Med Biol*. 2016;61(11):4327-4341. https://doi.org/10.1088/0031-9155/61/11/4327
81. Futami Y, Kanai T, Fujita M, et al. Broad-beam three-dimensional irradiation system for heavy-ion radiotherapy at HIMAC. *Nucl Instrum Methods Phys Res A Accel Spectrom Detect Assoc Equip*. 1999;430(1):143-153. https://doi.org/10.1016/S0168-9002(99)00194-1
82. Kanai T, Kanematsu N, Minohara S, et al. Commissioning of a conformal irradiation system for heavy-ion radiotherapy using a layer-stacking method. *Med Phys*. 2006;33(8):2989-2997. https://doi.org/10.1118/1.2219771
83. Diffenderfer ES, Verginadis II, Kim MM, et al. Design, Implementation, and in Vivo Validation of a Novel Proton FLASH Radiation Therapy System. *Int J Radiat Oncol Biol Phys*. 2020;106(2):440-448. https://doi.org/10.1016/j.ijrobp.2019.10.049
84. Simeonov Y, Weber U, Schuy C, et al. Monte Carlo simulations and dose measurements of 2D range-modulators for scanned particle therapy. *Z Med Phys*. 2021;31(2):203-214. https://doi.org/10.1016/j.zemedi.2020.06.008
85. Folkerts MM, Abel E, Busold S, Perez JR, Krishnamurthi V, Ling CC. A framework for defining FLASH dose rate for pencil beam scanning. *Med Phys*. 2020;47(12):6396-6404. https://doi.org/10.1002/mp.14456
86. Breneman J. Feasibility study of FLASH radiotherapy for the treatment of symptomatic bone metastases (FAST-01). *Nct04592887*. 2020:NCT04592887.
87. Zou W, Diffenderfer ES, Cengel KA, et al. Current delivery limitations of proton PBS for FLASH. *Radiother Oncol*. 2021;155:212-218. https://doi.org/10.1016/j.radonc.2020.11.002
88. van de Water S, Safai S, Schippers JM, Weber DC, Lomax AJ. Towards FLASH proton therapy: the impact of treatment planning and machine characteristics on achievable dose rates. *Acta Oncol (Madr)*. 2019;58(10):1463-1469. https://doi.org/10.1080/0284186X.2019.1627416.

How to cite this article: Weber UA, Scifoni E, Durante M. FLASH radiotherapy with carbon ion beams. *Med Phys*. 2022;49:1974–1992. https://doi.org/10.1002/mp.15135

APPENDIX

A1. OER calculation

The OER definition is in different publications misleadingly and ambiguously set; in the present work we define it in an original way, of "enhancement factor":

$$\mathrm{OER}\left(\mathrm{pO}_2, \mathrm{LET}\right) = D_{\mathrm{anoxia}}/D\left(\mathrm{pO}_2, \mathrm{LET}\right)|_{\text{same effect}},$$

While in different papers, it is expressed with the same symbol the quantity which we call

$$\overline{\mathrm{OER}}\left(\mathrm{pO}_2, \mathrm{LET}\right) = D\left(\mathrm{pO}_2, \mathrm{LET}\right)/D_{\mathrm{normox}}|_{\text{same effect}},$$

With the relation between the 2 being:

$$\begin{aligned}\mathrm{OER}(\mathrm{pO}_2, \mathrm{LET}) &= 1/\overline{\mathrm{OER}}(\mathrm{pO}_2, \mathrm{LET}) \cdot D_{\mathrm{anoxia}}/D_{\mathrm{normox}} \\ &= \overline{\mathrm{OER}}(0, \mathrm{LET})/\overline{\mathrm{OER}}(\mathrm{pO}_2, \mathrm{LET}).\end{aligned}$$

In Figure 3, both quantities are plotted.

A2. Amorphous track radius calculation

r_{90} and r_{80} in Figure 5 describe the extension of a particle track enclosing, respectively, 80% and 90% of the total dose and are derived by radial dose calculations according to the amorphous track model as in Ref. [60], by imposing

$$r_x : \int_0^{r_x} D(r) 2\pi r dr = x\,\% \frac{\mathrm{LET}}{\rho},$$

which, using the explicit formulation of the radial dose there defined, returns, for example:

$$r_{80} = r_{min} \exp\left[\frac{0.8\left(1 + 2\ln\left[\frac{r_{max}}{r_{min}}\right]\right) - 1}{2}\right],$$

where r_{max} is depending on the energy according to the Kiefer formula and r_{min} is the energy-dependent core radius.